mathematics

MDPI

Article

Non-Similarity Solutions of Non-Newtonian Brinkman–Viscoelastic Fluid

Siti Farah Haryatie Mohd Kanafiah [1], Abdul Rahman Mohd Kasim [2,*], Syazwani Mohd Zokri [3] and Nur Syamilah Arifin [4]

[1] Faculty of Computer and Mathematical Sciences, Universiti Teknologi MARA, Kelantan Branch, Machang 18500, Malaysia; sitif315@uitm.edu.my
[2] Centre for Mathematical Sciences, Universiti Malaysia Pahang, Gambang 26300, Malaysia
[3] Faculty of Computer and Mathematical Sciences, Universiti Teknologi MARA, Terengganu Branch, Kuala Terengganu 21080, Malaysia; syazwanimz@uitm.edu.my
[4] Faculty of Computer and Mathematical Sciences, Universiti Teknologi MARA, Johor Branch, Pasir Gudang 81570, Malaysia; nursyamilaharifin@uitm.edu.my
* Correspondence: rahmanmohd@ump.edu.my

Abstract: The exploration of heat transference in relation to fluid flow problems is important especially for non-Newtonian type of fluid. The use of the particular fluid can be found in many industrial applications such as oil and gas industries, automotives and manufacturing processes. Since the experimental works are costly and high-risk procedures, the mathematical study is proposed to counter the limitations. Therefore, this work aims to study the characteristics of a fluid that combines the properties of viscosity and elasticity, together with the porosity conditions, called the Brinkman–viscoelastic model. The flow is assumed to move over a horizontal circular cylinder (HCC) under consideration of the convective thermal boundary condition. The mathematical model is transformed to the less complex form by utilising a non-dimensionless and non-similarity variable. The resulting equations are in the partial differential equation (PDE) form. Subsequently, the equations are required to be solved by employing the Keller-box method (KBM). The solutions were conveniently evaluated by observing the plotted graphs in order to capture the propensity of the fluid's behavior in response to the adjusting parameters. The study discovered that the viscoelastic and Brinkman variables had the impact of decreasing the fluid's velocity and increasing the temperature distribution. Nevertheless, when mixed convection and Biot numbers increased, the velocity profile exhibited the opposite pattern. Furthermore, increasing the Biot number raises the Nusselt number while decreasing the skin friction coefficient. These numerical results are critical for assisting engineers in making heat transfer process decisions and accurately verifying experimental investigations.

Keywords: Brinkman model; porous region; convective boundary condition; horizontal circular cylinder; viscoelastic model

MSC: 76D05; 76D10; 35Q35; 76M20

Citation: Kanafiah, S.F.H.M.; Kasim, A.R.M.; Zokri, S.M.; Arifin, N.S. Non-Similarity Solutions of Non-Newtonian Brinkman–Viscoelastic Fluid. *Mathematics* **2022**, *10*, 2023. https://doi.org/10.3390/math10122023

Academic Editors: Ioannis Dassios and Clemente Cesarano

Received: 9 May 2022
Accepted: 9 June 2022
Published: 11 June 2022

1. Introduction

The boundary layer theory is very useful for tackling problems involving the movement of two important elements, which are fluid and heat. When a real fluid flows across a stationary solid boundary, the viscous force exerts a significant influence on the velocity and thermal boundary layers [1]. To address expanding issues in technology and engineering applications, a growing number of mathematicians are focusing on the study of convective boundary flow of non-Newtonian types of fluid. As per Jaiswal [2], the existence of the mentioned fluid happened when a fluid is subjected to shear stress, resulting in rotation and shrinkage. Recently, there has been interest in convective flow problems involving

various geometry and boundary conditions, for instance, the flow along a flat plate [3,4], over an HCC [5,6] and over a sphere [7,8].

The mixed convection flow was investigated in this paper due to its potential in industrial applications and engineering devices such as heating and cooling in channel flows. In particular, this flow results from the mutual reaction between natural and forced convections, on which the variation in surface temperature happens. Through a theoretical investigation, Acrivos et al. [9] were pioneers in the analysis of flow behavior associated with a mixed convection effect for the case of the broad section of the body at a stagnation point. Merkin et al. [10] analysed the flow in both situations of heated-cooled cylinders via numerical integration approach and series expansion. The outcomes showed the boundary layer separation suppressed in the range of $0^{\circ} < x < 180^{\circ}$. Ali et al. [11] deliberated on the convective fluid with microrotation and revealed that for opposing flow, the separation time is postponed at the stagnation point, but for assisting flow, this does not occur. In the geometry of HCC, Kasim et al. [12] presented the solution for the motion of viscoelastic fluid flow by highlighting the heat production features. The results suggested that the movement and heat transmission characteristics were impacted by the viscoelastic parameter, along with heat production. Zokri et al. [13] explored the viscous dissipation impact in a Jeffrey fluid flow across an HCC. The Jeffrey fluid parameter demonstrated inconsistent behaviour for velocity and temperature distribution. The study was repeated the following year by Zokri et al. [14] utilising Jeffrey nanofluid. They noticed that raising the Eckert number resulted in a slight change in the physical quantities of flow. Nevertheless, at the cylinder's stagnation point, the Eckert number has little influence on both velocity and temperature profiles. Mahat et al. [15] offered research on the flow of viscoelastic embedded with nanofluid and the presence of a viscous dissipation effect. The heat transfer coefficient is judged to be more successful and considerable at the stagnation point due to the principal heat source at the boundary conditions. Basha et al. [16] considered the investigation on fluid transport characteristics by embedding the entropy generation towards the tangent hyperbolic nanofluids. Higher levels of mixed convection increase overall entropy production and improve thermal convection parameters.

The porous medium has been taken into account in this work. There are numerous papers in the literature that discuss convective flow in porous media [17–19]. The Brinkman model, according to Alrabaiah et al. [20], elaborates on the fluid flowing in a high- porosity incompressible surface. Due to the extensive applications in the porosity field, such as grain storage, electronic devices and petroleum reservoirs, numerous studies have been conducted using the Brinkman model. Brinkman's pioneering work in 1949 [21] contributed a model employed in large holey surfaces. This scientist applied the Navier Stoke's formula to study the flow triggered by the viscous force of minuscule spheres. Varma and Babu [22] investigated the flow over a porous channel under the effect of a magnetic field. The problem of nanofluid occupying a sphere saturated in a porous medium by using the Brinkman model in two flow cases was examined by Tham and Nazar [23]. Considering the effect of mixed convection, the solution for aiding and opposing flow was obtained. They found that increasing the mixed convection parameter delays and suppresses boundary layer separation in the range $0^{\circ} < x < 120^{\circ}$. Yadav [24] examined the onset of convection in a Darcy–Brinkman fluid and exposed that the Darcy number and gravitational forces were deferred during convection. In addition, Rafique et al. [25] inspected the motion of the fluid on Brinkman micropolar nanofluid and highlighted that the velocity of the fluid reduces as the Brinkman parameter increases.

Another aspect influencing fluid flow heat transfer is the thermal boundary condition. The fact that the heat transfer surfaces are bared to a convective atmosphere at stated parameters means that the convective boundary condition (CBC) is likely the most often-found boundary condition in practice. Convective boundary condition represents the contact of detour wall conduction with the thermal film, which caused heated fluid and impacted heat exchange efficiency. In the context of CBC, Alkasasbeh et al. [26] explored the flow of a combined convection effect through a solid sphere. They found that raising

the conjugate parameter reduces the thermal characteristics of the fluid. Moreover, the investigation of the boundary layer flow was addressed by Ramesh et al. [27] in the case of the moving flat plate. When a thermal gradient was given to the surface, the ratio regulating the temperature inside a body altered dramatically. Sarif et al. [28] investigated the influence of CBC set up in viscous fluid flowing through HCC. The same authors then extended their study for nanofluid flow, as documented in Sarif et al. [29]. In another paper, Ashraf et al. [30] studied the effect of CBC on mixed convection boundary layer flow of Casson fluid over a stretched sheet with Hall Effect. The author discovered that increasing the conjugate parameter improves thermal characteristics. Eventually, Mahat et al. [31] numerically investigated the steady mixed convection flow of a viscoelastic nanofluid under the effect of heat generation. They concluded that when the Biot number upsurges, the fluid distributions are also increased.

As an outcome of the research conducted, a new model of fluid flow has been proposed. This study extended the basics of the Brinkman model to Brinkman–viscoelastic fluid in conjunction with viscoelastic knowledge. As a consequence, this study addresses mixed convective flow on an HCC of Brinkman-viscoelastic fluid immersed in a porous medium under the effects of CBC. The numerical results are attained using the KBM encoded in MATLAB R2019a software. The flow and heat transmission properties are examined and analysed for various values of the Biot number, mixed convection, Brinkman and viscoelastic factors. The proposed theoretical model enables it to investigate the problem of heat transfer in the porous region with viscosity and elasticity characteristics such as the filtration process of blood through a membrane, oil reservoir engineering and material processing. The provided theoretical results will aid the engineers to make a better decision in the heat transfer process in order to generate high-quality products.

2. Problem Formulation

Referring to Tonekobani et al. [32], the variables of Cauchy stress tensor for viscoelastic model are adopted as

$$\boldsymbol{\tau} = -\overline{p}\mathbf{I} + 2\mu_0\mathbf{d} - 2k_0\overset{\nabla}{\mathbf{d}} \tag{1}$$

Here, $\mathbf{I}$, $\mathbf{d}$, $\overset{\nabla}{\mathbf{d}}$, μ_0 and k_0 are declared as identity tensor, deformation rate tensor, upper-convected derivative, dynamic viscosity and the short-memory coefficient, respectively. Next, the variable upper-convected derivative of tensor is defined as

$$\overset{\nabla}{\mathbf{d}} = (\mathbf{V}\cdot\nabla)\mathbf{d} - \mathbf{d}\cdot(\nabla\mathbf{V})^{tr} - \nabla\mathbf{V}\cdot\mathbf{d} \tag{2}$$

The above constitutive equation is used to obtain the boundary layer equation. This study deals with the laminar and steady mixed convection flow of a viscoelastic mode together with the Brinkman concept. Figure 1 depicts the physical configuration and fluid flow pattern, where the fluid is flowing through HCC in a porous medium. In a rectangular system, $\overline{x}$ is calculated along the cylinder and $\overline{y}$ is regarded perpendicular to the cylinder. $\frac{1}{2}U_\infty$ declared as velocity at free stream is assumed to move upward through the cylinder under the gravitational acceleration g where T_∞ is the surrounding temperature. For thermal boundary condition of CBC, it is stated that T_f is the temperature when convection heats the cylinder's surface from hot fluid, h_f is a heat transfer coefficient and k is the thermal conductivity.

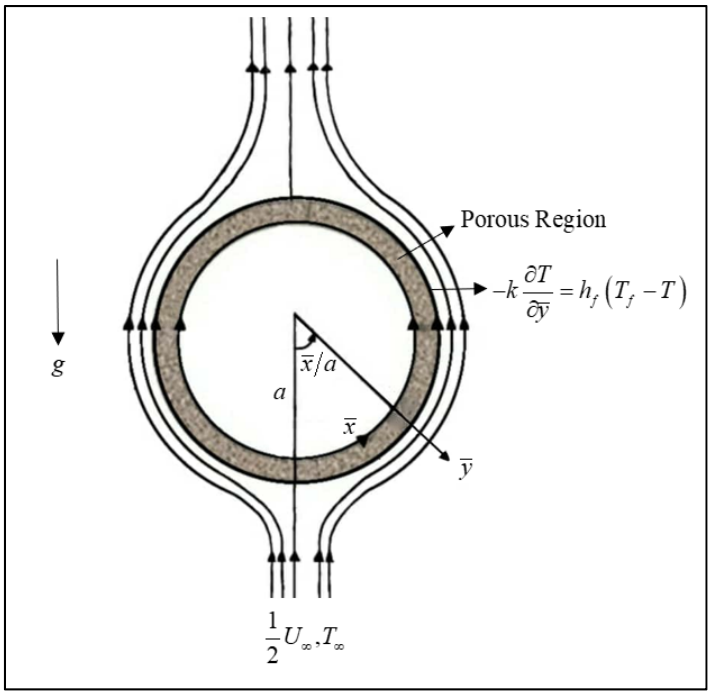

Figure 1. Fluid flow pattern through cylinder surface.

The updated fluid model by Refs. [33,34] consists of continuity, momentum and energy equations under Boussinesq and boundary layer assumptions as follows

$$\frac{\partial \overline{u}}{\partial \overline{x}} + \frac{\partial \overline{v}}{\partial \overline{y}} = 0, \tag{3}$$

$$\begin{aligned} \frac{\mu}{K}\,\overline{u} = \; & \frac{\mu}{\phi}\,\frac{\partial^2 \overline{u}}{\partial \overline{y}^2} + \overline{u}_e \frac{\partial \overline{u}_e}{\partial \overline{x}} + k_0\left[\overline{u}\,\frac{\partial^3 \overline{u}}{\partial \overline{x}\partial \overline{y}^2} + \overline{v}\frac{\partial^3 \overline{u}}{\partial \overline{y}^3} - \frac{\partial \overline{u}}{\partial \overline{y}}\,\frac{\partial^2 \overline{u}}{\partial \overline{x}\partial \overline{y}} + \frac{\partial \overline{u}}{\partial \overline{x}}\,\frac{\partial^2 \overline{u}}{\partial \overline{y}^2}\right] \\ & + \rho g \beta (T - T_\infty)\,\sin\left(\tfrac{\overline{x}}{a}\right), \end{aligned} \tag{4}$$

$$\overline{u}\frac{\partial T}{\partial \overline{x}} + \overline{v}\frac{\partial T}{\partial \overline{y}} = \alpha_m \frac{\partial^2 T}{\partial \overline{y}^2}. \tag{5}$$

with the referred boundary conditions

$$\begin{aligned} & \overline{v} = 0,\ \overline{u} = 0,\ -k\tfrac{\partial T}{\partial \overline{y}} = h_f\left(T_f - T\right) \text{ at } \quad \overline{y} = 0, \\ & \overline{u} \to \overline{u}_e(\overline{x}),\ \overline{v} \to 0,\ T \to T_\infty \text{ as } \quad \overline{y} \to \infty. \end{aligned} \tag{6}$$

The velocity along $\overline{x}$ and $\overline{y}$ directions are defined as $\overline{u}$ and $\overline{v}$ in the governing model, respectively. In addition, the external velocity flow is referred to as $\overline{u}_e(\overline{x}) = U_\infty \sin(\overline{x}/a)$.

By introducing the non-dimensional boundary layer variables from Ref. [35] as follows,

$$\begin{aligned} & x = \overline{x}/a,\ y = Pe^{1/2}\,(\overline{y}/a),\ u = \overline{u}/U_\infty,\ v = Pe^{1/2}\,(\overline{v}/U_\infty), \\ & \theta = (T - T_\infty)/(T_f - T_\infty),\ u_e(\overline{x}) = \overline{u}_e(\overline{x})/U_\infty, \end{aligned} \tag{7}$$

the PDEs (3) to (6) are transformed into a non-dimensional form, where $Pe = U_\infty a/\alpha_m$ is a modifed Péclet number and yields to

$$\frac{\partial u}{\partial x} + \frac{\partial v}{\partial y} = 0, \tag{8}$$

$$\frac{\partial u}{\partial y} = \Gamma \frac{\partial^3 u}{\partial y^3} + k_1 \left[\begin{array}{l} u\frac{\partial^4 u}{\partial x \partial y^3} + \frac{\partial^3 u}{\partial x \partial y^2}\frac{\partial u}{\partial y} + v\frac{\partial^4 u}{\partial y^4} + \frac{\partial^3 u}{\partial y^3}\frac{\partial v}{\partial y} - \frac{\partial u}{\partial y}\frac{\partial^3 u}{\partial x \partial y^2} \\ -\frac{\partial^2 u}{\partial x \partial y}\frac{\partial^2 u}{\partial y^2} + \frac{\partial u}{\partial x}\frac{\partial^3 u}{\partial y^3} + \frac{\partial^2 u}{\partial y^2}\frac{\partial^2 u}{\partial x \partial y} \end{array} \right] + \lambda \frac{\partial \theta}{\partial y} \sin x, \quad (9)$$

$$u\frac{\partial \theta}{\partial x} + v\frac{\partial \theta}{\partial y} = \frac{\partial^2 \theta}{\partial y^2} \quad (10)$$

subjected to the transformed boundary condition

$$\begin{array}{l} u = 0,\ v = 0,\ \frac{\partial \theta}{\partial y} = -Bi(1-\theta) \text{ at } \ \overline{y} = 0, \\ u \to u_e,\ v \to 0,\ \theta \to 0 \text{ as } \ \overline{y} \to \infty. \end{array} \quad (11)$$

The following non-similarity transformation variables are used and have satisfied the Equation (8),

$$\psi = x\, f(x,y),\ \theta = \theta(x,y), u = \frac{\partial \psi}{\partial y}, v = -\frac{\partial \psi}{\partial x}, \quad (12)$$

where ψ and θ are defined as the stream function and fluid temperature, accordingly. Hence, by substituting Equation (12) to the Equations (9)–(11), the following systems are attained

$$\begin{array}{l} f' - \Gamma f''' \ - k_1\left[2f'f''' - ff^{(iv)} - (f'')^2\right] - (1+\lambda\theta)\ \frac{\sin x}{x} = \\ xk_1\left[f'\frac{\partial f'''}{\partial x} - \frac{\partial f}{\partial x}f^{(iv)} - f''\frac{\partial f''}{\partial x}^2 + \frac{\partial f'}{\partial x}f'''\right] \end{array} \quad (13)$$

$$\theta'' + f\,\theta' = x\left(f'\frac{\partial \theta}{\partial x} - \frac{\partial f}{\partial x}\,\theta'\right). \quad (14)$$

$$\begin{array}{l} f(0) = 0, \quad f'(0) = 0, \quad \theta'(0) = -Bi(1-\theta), \\ f'(\infty) \to \frac{\sin x}{x}, \quad f''(\infty) \to 0, \quad \theta(\infty) \to 0 \end{array} \quad (15)$$

Note that $(')$ is the derivative term of y. The physical parameters involved in Equation (13) are declared as $\Gamma = \frac{Da}{\phi}Pe$, $\lambda = \frac{Ra}{Pe}$ and $k_1 = \frac{k_0 K U_\infty Pe}{\mu a^3}$. Further, the non-dimensional variables are demarcated as $Da = \frac{K}{a^2}$ and $Ra = \frac{gK\beta(T_w - T_\infty)a}{\alpha_m v}$. The detailed formulation steps of the momentum equation starting from Equation (4) are provided in Appendix A.

The PDEs (13) to (15) are converted to the less complex form (at lower stagnation region of the cylinder ($x \approx 0$)),

$$f' - \Gamma f''' \ - k_1\left[2f'f''' - ff^{(iv)} - (f'')^2\right] - 1 - \lambda\theta = 0, \quad (16)$$

$$\theta'' + f\,\theta' = 0. \quad (17)$$

subjected to boundary condition

$$\begin{array}{l} f(0) = 0, \quad f'(0) = 0, \quad \theta'(0) = -Bi(1-\theta), \\ f'(\infty) \to 1, \quad f''(\infty) \to 0, \quad \theta(\infty) \to 0. \end{array} \quad (18)$$

The reduced physical quantities which were once mentioned by [33] are as follows

$$C_f Pe^{1/2}/\mathrm{Pr} = x\frac{\partial^2 f}{\partial y^2}, \quad NuPe^{-1/2} = -\frac{\partial \theta}{\partial y}. \quad (19)$$

3. Numerical Procedures

The KBM is employed to solve the PDEs (13) to (15). This method is found to have unconditional stability, offers rapid convergence, is suitable for solving non-linear parabolic differential equations and can be modified to solve problems of any order [36].

The dependent variables in Equations (13) and (14) are transformed to a first-order system as presented below

$$f' = u, \quad u' = v, \quad v' = p, \quad s' = t. \tag{20}$$

Thus, Equation (13) together with (14) are then transformed into

$$u - \Gamma p \; - k_1 \left[2up - fp' - v^2 \right] - (1 + \lambda s) \, \frac{\sin \, x}{x} = x k_1 \left[u \frac{\partial p}{\partial x} - \frac{\partial f}{\partial x} p' - v \frac{\partial v}{\partial x} + \frac{\partial u}{\partial x} p \right], \tag{21}$$

$$t' + \; ft \; = x \left(u \frac{\partial s}{\partial x} \; - \; \frac{\partial f}{\partial x} \, t \right). \tag{22}$$

and Equation (15) becomes

$$\begin{array}{l} u = 0, \quad f = 0, \quad t = -Bi(1 - s) \quad \text{at } y = 0, \\ u \to \frac{\sin x}{x}, \quad v \to 0, \quad s \to 0 \quad \text{as } y \to \infty. \end{array} \tag{23}$$

Four steps are involved in the numerical technique process as shown in Figure 2. For the first step, a first-order system yielding from the simplification of PDEs is obtained. The achieved system is then written in finite-difference form with central differences. The finite difference is then linearised and converted to a matrix-vector form using Newton's method. Finally, the method of blocking tridiagonal elimination provides the solution for the resulting system.

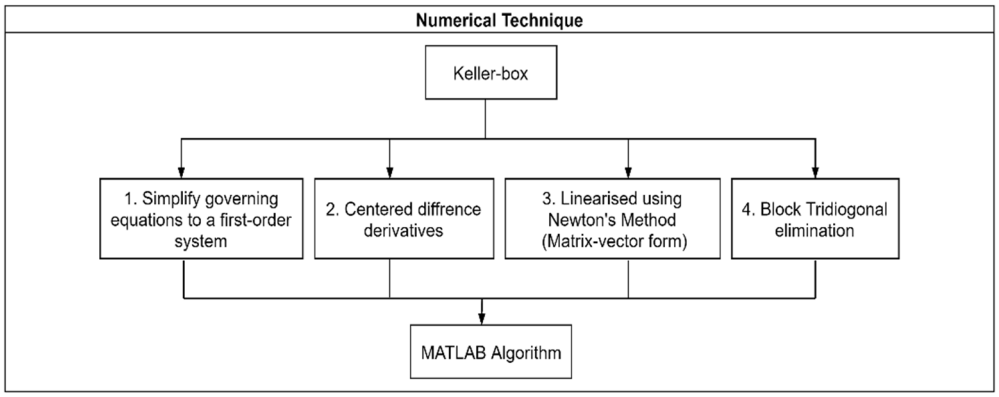

Figure 2. Diagram for KBM.

4. Validation Procedure

The algorithm is built from the KBM using MATLAB computational tools in order to analyse the characteristics of various physical variables existing in the final equation of the proposed model. The step size $\Delta y = 0.02$, $\Delta x = 0.01$ and the boundary layer thickness of $y_\infty = 8$ are used to ensure the results asymptotically meet the applied conditions. In a few limited cases, the current model is confirmed by relating the value of the skin friction coefficient to previously published outputs. The fixed parameters of $\Gamma = 0.1$, $k_1 = 0$, $\lambda = 1$ and $Bi \to \infty$ are used, except otherwise stated. The current findings agree with Nazar et al. [33] and Tham et al. [35] as shown in Table 1. Table 2 also shows the comparison of momentum equations with the work carried out by Nazar et al. [33] and Tham et al. [35]. As a result, the proposed model is appropriate for further investigation.

Table 1. Comparative value of $C_f Pe^{1/2}/\mathrm{Pr}$ at $\Gamma = 0.1$, $Bi \to \infty$ and $k_1 = 0$.

x	$\lambda = 1$		
	Nazar et al. [33]	**Tham et al. [35]**	**Current**
0.2	1.1101	1.1115	1.111488
0.6	3.1573	3.1696	3.169580
0.8	4.0175	4.0387	4.038699
1.0	4.7234	4.7555	4.755531
1.2	5.2477	5.2921	5.292116
1.6	5.6736	5.7447	5.744702

Table 2. Comparative model in terms of momentum equations.

Author	Model (Momentum)	Limiting Cases
Current	$f' - \Gamma f''' - k_1\left[2f'f''' - ff^{(iv)} - (f'')^2\right] - (1+\lambda\theta)\,\frac{\sin x}{x} = xk_1\left[f'\frac{\partial f'''}{\partial x} - \frac{\partial f}{\partial x}f^{(iv)} - f''\frac{\partial f''}{\partial x}^2 + \frac{\partial f'}{\partial x}f'''\right]$	$k_1 = 0$
Nazar et al. [33]	$f' - \Gamma f''' - (1+\lambda\theta)\,\frac{\sin x}{x} = 0$	-
Tham et al. [35]	$f' - \Gamma f''' - (1+(\theta - Nr\varphi)\lambda)\,\frac{\sin x}{x} = 0$	$Nr = 0$

5. Results and Discussion

In this research, the value of the viscoelastic parameter k_1 is taken as a non-negative parameter k_1 since the study is aiming to investigate the outcome of the presence of viscosity and elasticity properties. Therefore, the value of k_1 must be greater than zero to show the effect of viscoelastic properties. It is worth mentioning that the value of $k_1 \geq 8$ is chosen for the entire analysis. Furthermore, the mixed convection parameter, $\lambda > 0$ shows the assisting flow and $\lambda < 0$ represents the opposing flow. To characterise the Brinkman factor, $\Gamma > 0$ is scrutinised due to the effect of porosity variation. The values for the Biot number are used within the range $0.05 \leq Bi \leq 0.2$. Physically, there are no meaningful impacts on the boundaries when the large value of Bi is employed. Figures 3–10 show the velocity and temperature distributions at the stagnation point ($x \approx 0$) for different values of k_1, λ, Γ and Bi. Figures 3 and 4 are plotted against velocity and temperature profiles to demonstrate the fluid's characteristics. It is noticeable that the distribution of velocity, $f'(y)$, reduces while the temperature, $\theta(y)$, intensifies with the greater value of k_1. Physically, this is due to both viscous and elastic properties resulting in the resistant motion of the fluid. Therefore, the temperature profile increases because of the convection process. Next, Figures 5 and 6 show the variation in $f'(y)$ and $\theta(y)$ when the value of λ changes. According to the figure, as the value of λ rises, the $f'(y)$ increases but $\theta(y)$ decreases. This happens because buoyancy forces dominate the flow direction, causing the fluid to accelerate and the velocity profiles to rise. However, the convection process at the cylinder's surface causes the heat transfer rate to increase, gradually decaying the temperature profile. Figure 7 depicts the effect of Γ when compared with the velocity distribution. From the figure, a decreasing trend in $f'(y)$ is observed corresponding to the increase in Γ. Since the Brinkman parameter represents the porosity in porous media, the drag force raises as the Γ increases, resulting in a decrease in velocity [37]. Meanwhile, as shown in Figure 8, the $\theta(y)$ behaves in the opposite direction as the Γ increases. Furthermore, Figures 9 and 10 show how the various Bi affect the fluid velocity and temperature profiles. In general, the Biot number is represented by convection followed by conduction at the surface of the cylinder. Analysis gained in Figure 10 shows that $f'(y)$ slightly increases as the Bi increases due to convective heat transfer in cylinder surface. The $\theta(y)$ is also increased with an increase in Bi in Figure 10. Physically, a higher Biot number present strong surface convection, which stores supplementary heat to the surface. Figures 11 and 12 present the local skin friction and Nusselt number towards the Biot number. From the figure, it is clear that the $C_f Pe^{1/2}/\mathrm{Pr}$ is reduced and $NuPe^{-1/2}$ is inflated with the increment of Bi. The increase in the Biot number may exert the convective heat transference originating from the hot fluid to the cold surface of the cylinder that causes the increase in the heat transfer rate.

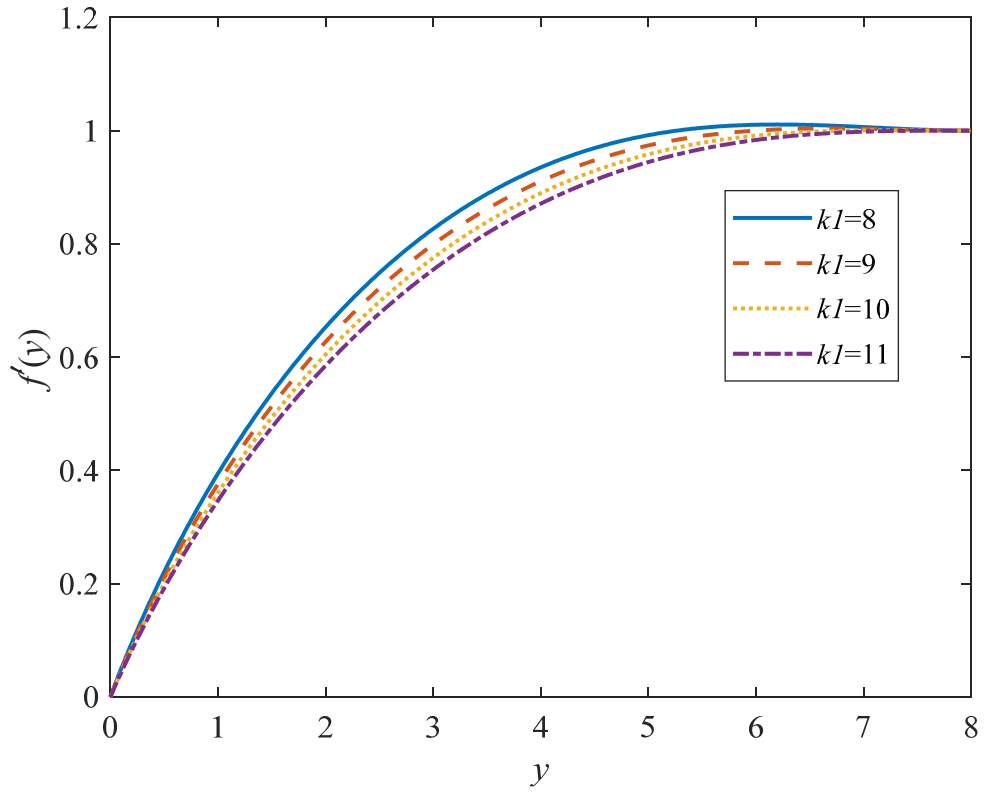

Figure 3. Effect of k_1 on $f'(y)$ when $\Gamma = 0.1$, $\lambda = 1$ and $Bi = 0.1$.

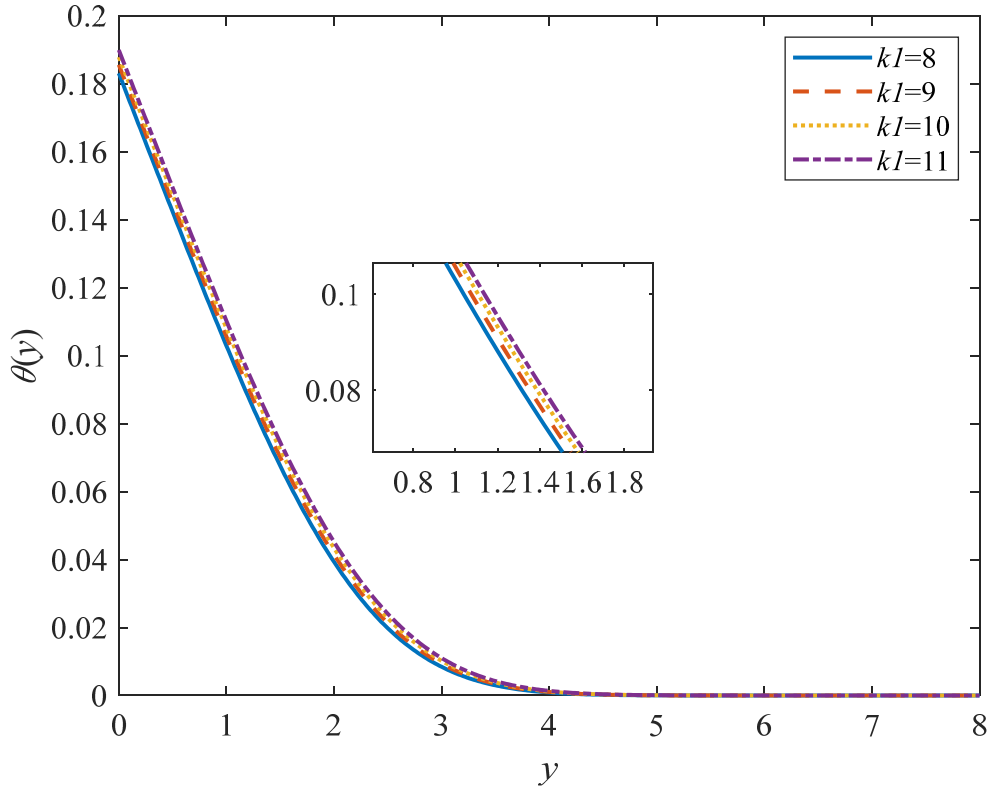

Figure 4. Effect of k_1 on $\theta(y)$ when $\Gamma = 0.1$, $\lambda = 1$ and $Bi = 0.1$.

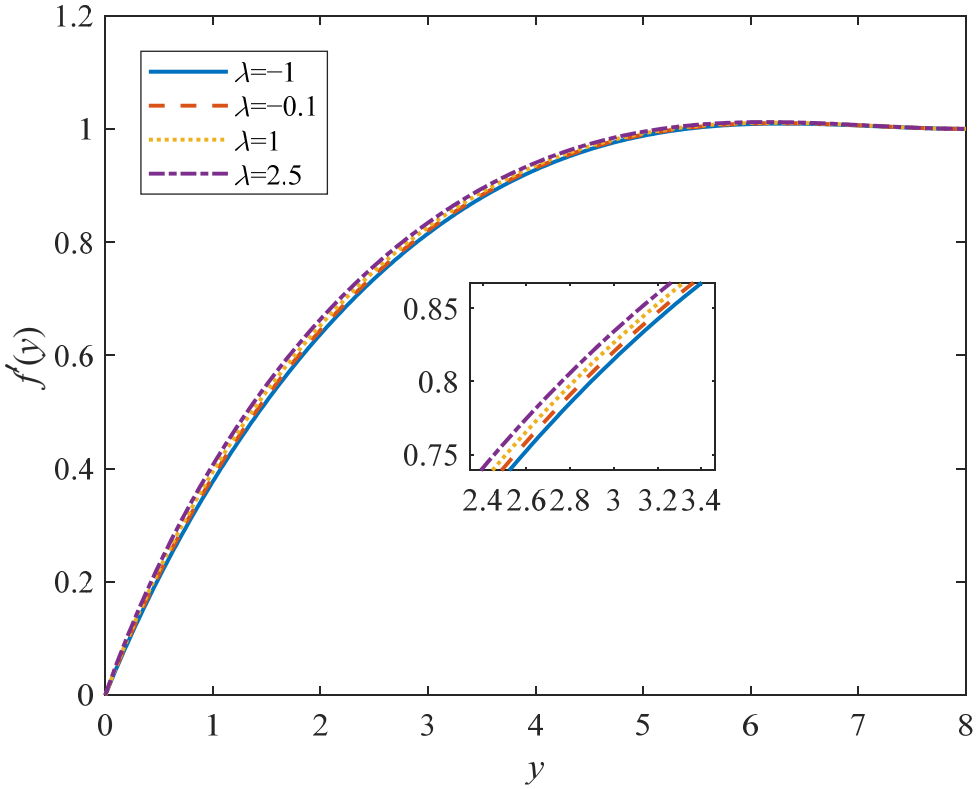

Figure 5. Effect of λ on $f'(y)$ when $\Gamma = 0.1$, $k_1 = 8$ and $Bi = 0.1$.

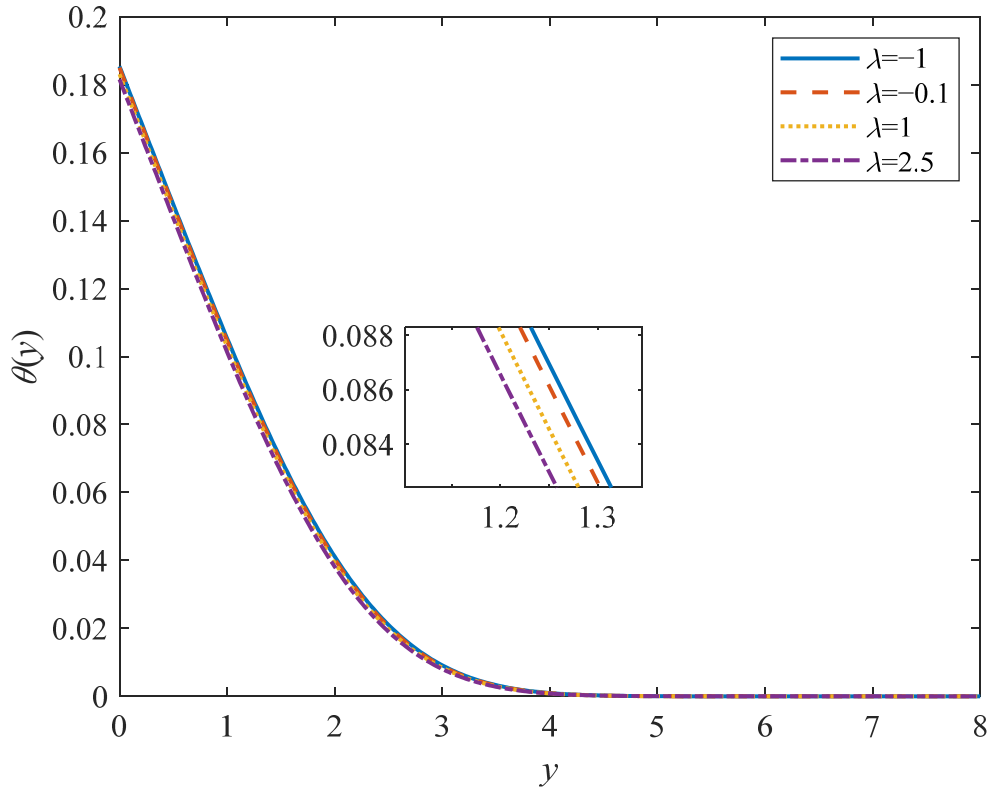

Figure 6. Effect of λ on $\theta(y)$ when $\Gamma = 0.1$, $k_1 = 8$ and $Bi = 0.1$.

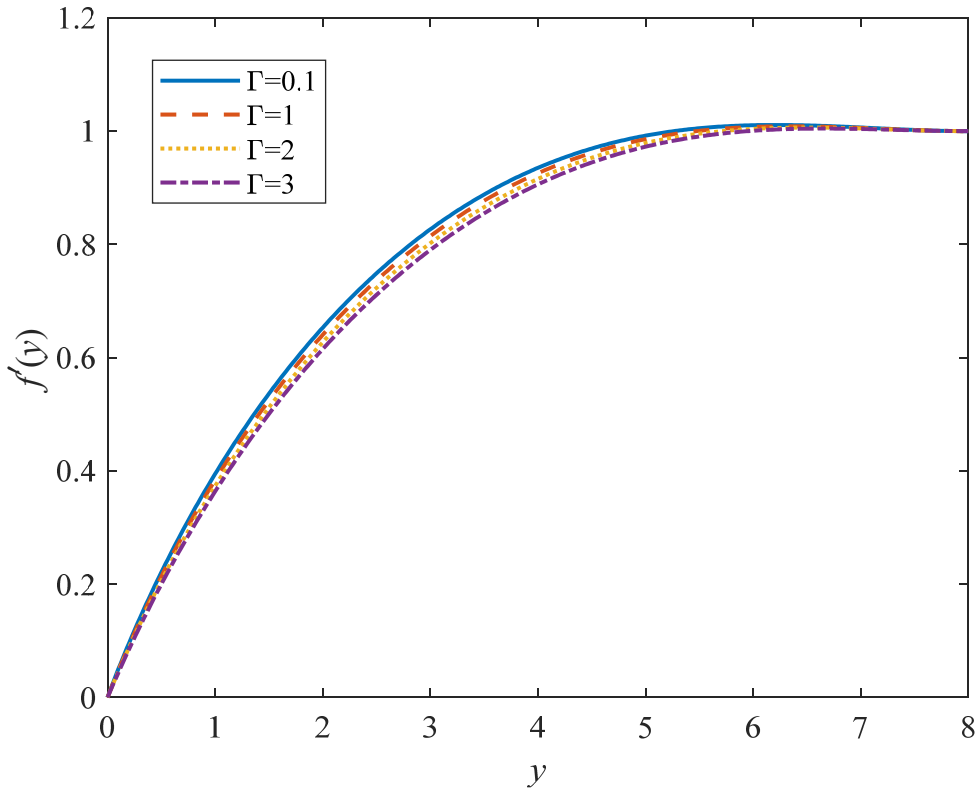

Figure 7. Effect of Γ on $f'(y)$ when $\lambda = 1$, $k_1 = 8$ and $Bi = 0.1$.

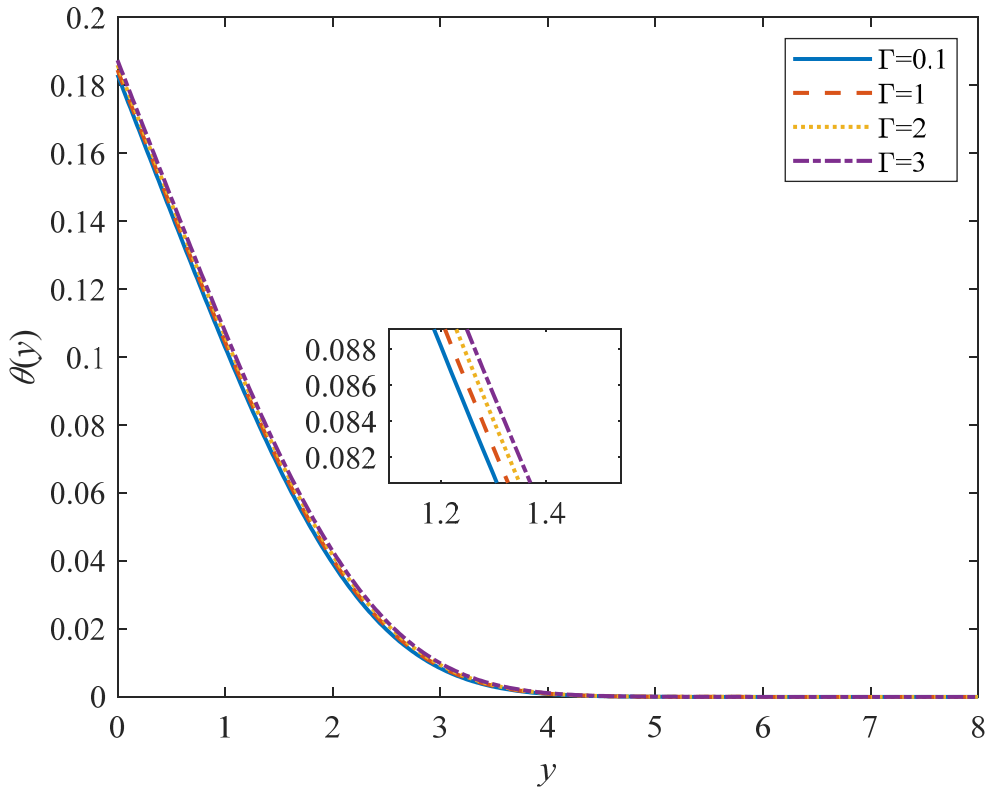

Figure 8. Effect of Γ on $\theta(y)$ when $\lambda = 1$, $k_1 = 8$ and $Bi = 0.1$.

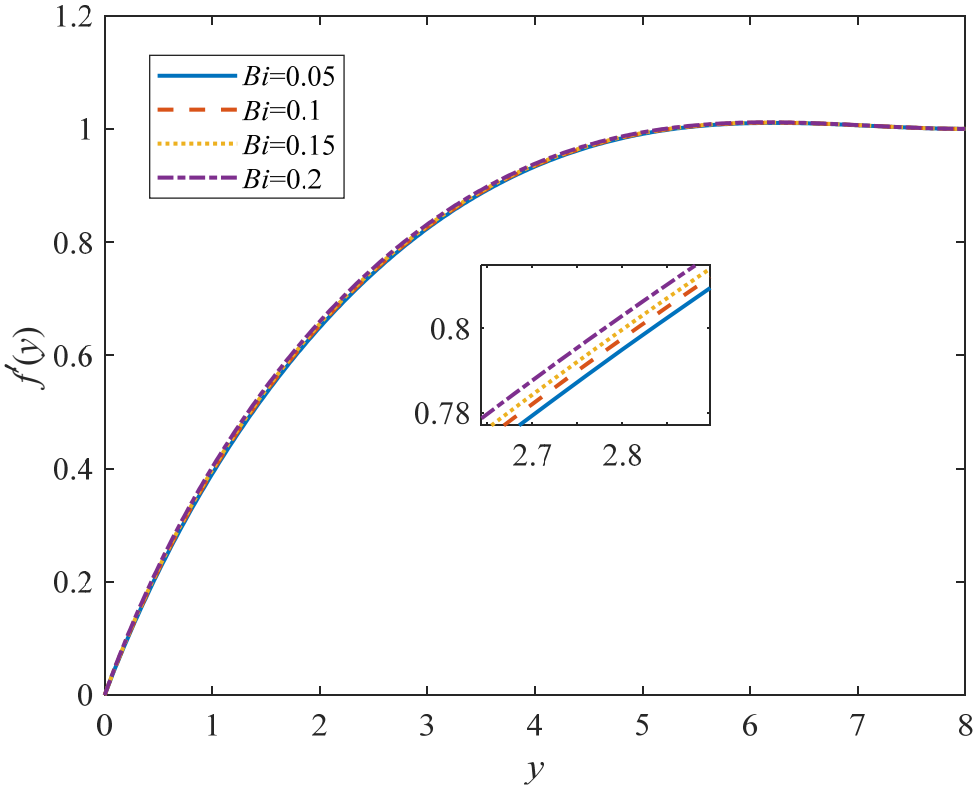

Figure 9. Effect of Bi on $f'(y)$ when $\lambda = 1$, $k_1 = 8$ and $\Gamma = 0.1$.

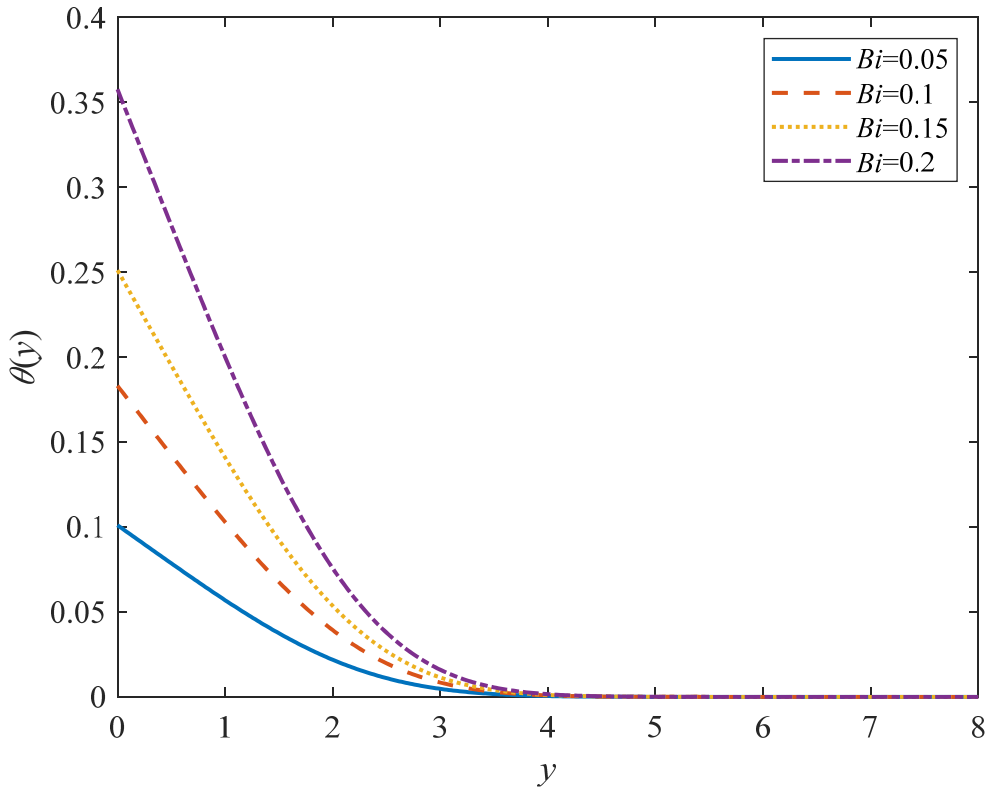

Figure 10. Effect of Bi on $\theta(y)$ when $\lambda = 1$, $k_1 = 8$ and $\Gamma = 0.1$.

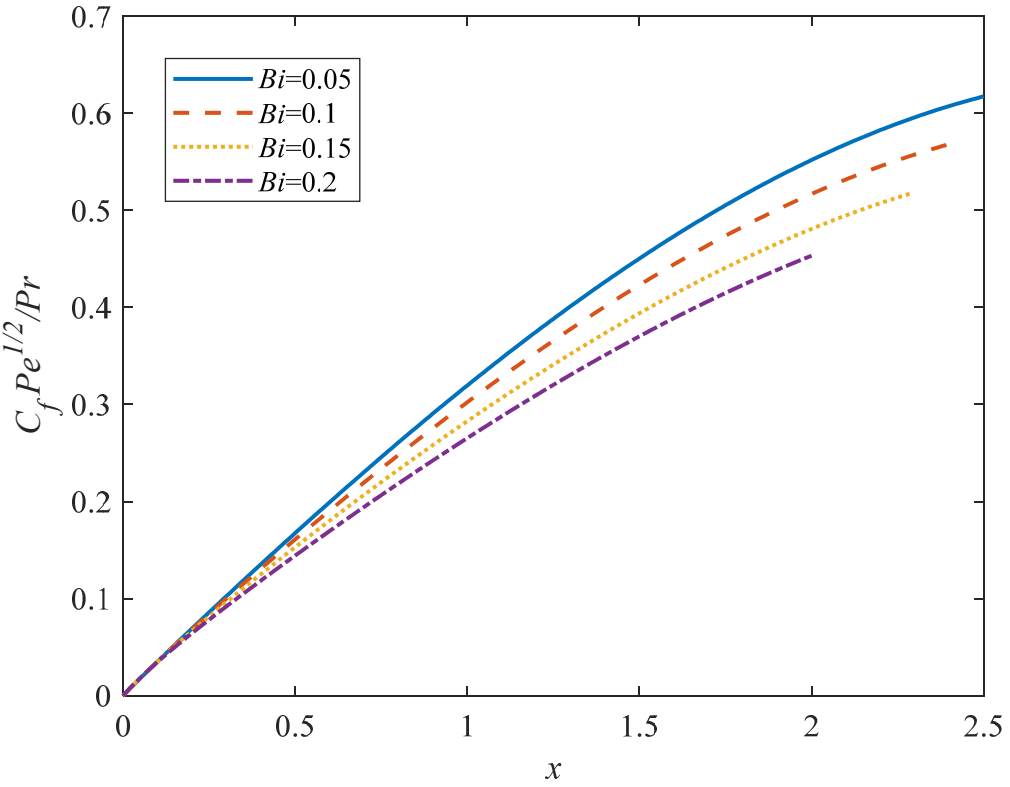

Figure 11. Effect of Bi on $C_f Pe^{1/2}/\mathrm{Pr}$ when $\lambda = 1$, $k_1 = 8$ and $\Gamma = 0.1$.

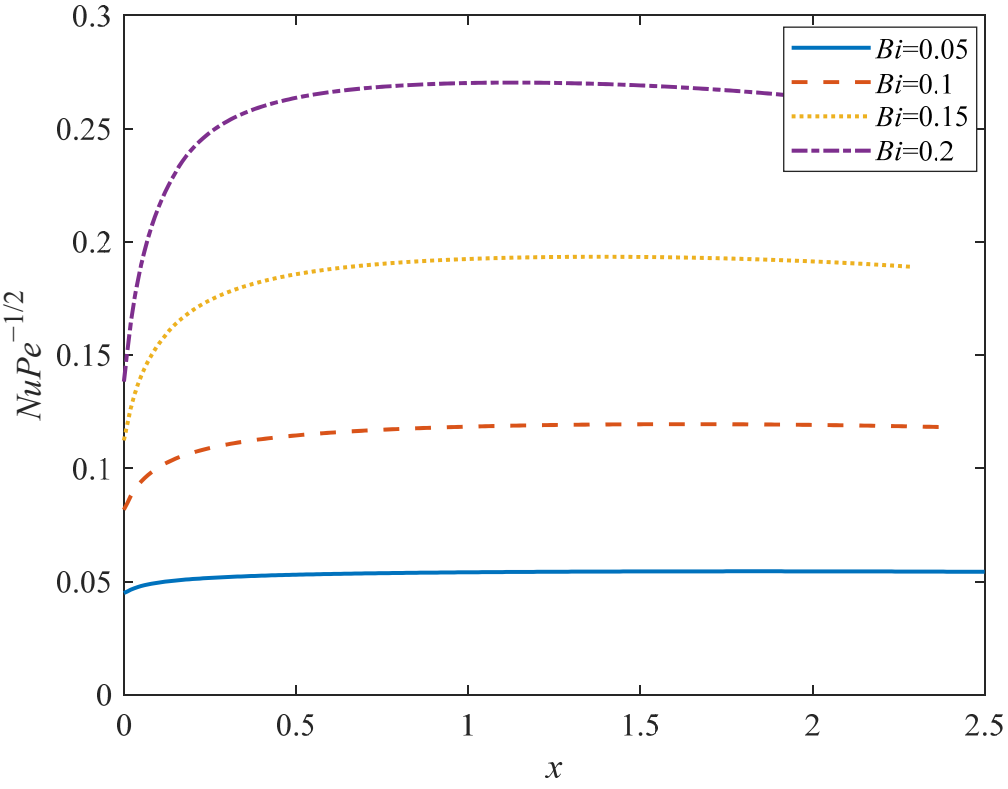

Figure 12. Effect of Bi on $NuPe^{-1/2}$ when $\lambda = 1$, $k_1 = 8$ and $\Gamma = 0.1$.

6. Conclusions

The exploration of a Brinkman–viscoelastic fluid flowing across HCC by considering combined convective transport is presented. The analysis considered the heating process as the convective boundary condition. By including relevant non-dimensional and non-similarity transformation variables into the governing equations, which include continuity, momentum and energy equations, a dimensionless form of PDEs may be created. The numerical solutions are computed using the KBM and Matlab software. The results are compared with previously published articles in order to validate the proposed model. As a result, the numerical solutions show perfect agreement, indicating that the proposed model and method are appropriate for further investigation. In conclusion, all of the parameters investigated in this study have a significant influence on fluid flow behaviours and can be recapitulated as follow:

1. It is observed that the viscoelastic and Brinkman parameter reduces the velocity profile whereas the mixed convection parameter enhances the velocity profile.
2. The Biot number elevates the velocity and temperature profiles.
3. The Brinkman and viscoelastic parameter increases the temperature profile, whereas it can be decreased by enlarging the mixed convection parameter.
4. The Biot number significantly diminishes the skin friction coefficient and elevates the Nusselt number.

Author Contributions: Conceptualization, S.M.Z. and N.S.A.; methodology, S.F.H.M.K.; validation, A.R.M.K.; writing—original draft, S.F.H.M.K. and A.R.M.K.; review and editing, S.M.Z. and N.S.A. All authors have read and agreed to the published version of the manuscript.

Funding: This project has been supported by Universiti Teknologi MARA Kelantan (600-TNCPI 5/3/DDN(03)(004/2021)).

Acknowledgments: The authors wish to thank Universiti Teknologi MARA Kelantan for the financial support through (600-TNCPI 5/3/DDN(03)(004/2021)). Our heartfelt thanks also go to Universiti Malaysia Pahang (RDU213204) for their assistance and support.

Conflicts of Interest: The authors declare that they have no conflicts of interest to report regarding the present study.

Nomenclature

a	radius of cylinder	$C_f Pe^{1/2}/\mathrm{Pr}$	local skin friction coefficient
U_∞	free-stream velocity	$NuPe^{-1/2}$	reduced Nusselt number
T_f	hot fluid temperature	Ra	Rayleigh number
T_∞	ambient temperature	Da	Darcy number
h_f	heat transfer coefficient	y	Boundary layer thickness
g	gravitational acceleration	Greek Symbols	
$\overline{x}, \overline{y}$	coordinate surface	ϕ	porosity of porous medium
$\overline{u}, \overline{v}$	velocity in $\overline{x}$, $\overline{y}$-directions	μ	dynamic viscosity
K	permeability	β	thermal-expansion coefficient
k_1	viscoelastic parameter	α_m	effective thermal diffusivity of porous
T	fluid temperature	ψ	stream function
k	thermal conductivity	θ	fluid temperature
$\overline{u}_e(\overline{x})$	external velocity	Γ	Brinkman parameter
Bi	Biot number	v	kinematic viscosity
Pe	modified Péclet number	λ	Mixed-convection parameter

Appendix A

Problem formulation of momentum equation

Non-dimensional variables

From Equation (4), apply boundary layer variables (7), yielded

$$\begin{aligned}\frac{\mu}{K}(uU_\infty) = \frac{\mu U\infty}{\phi a^2} Pe\frac{\partial^2 u}{\partial y^2} + U_\infty \sin x\frac{\partial(U_\infty \sin x)}{\partial \overline{x}} + \\ k_0\frac{U_\infty{}^2}{a^3}\left[Pe\, u\frac{\partial^3 u}{\partial x\partial y^2} + Pe\, v\frac{\partial^3 u}{\partial y^3} - Pe\frac{\partial u}{\partial y}\frac{\partial^2 u}{\partial x\partial y} + Pe\frac{\partial u}{\partial x}\frac{\partial^2 u}{\partial y^2}\right] + \rho\beta\theta(T_w - T_\infty)g\ \sin\ x,\end{aligned} \tag{A1}$$

Then, multiply (A1) by $\frac{K}{\mu U_\infty}$ and define the dimensionless parameter as $\Gamma = \frac{Da}{\phi}Pe$, $\lambda = \frac{Ra}{Pe}$, $v = \frac{\mu}{\rho_\infty}$ and $k_1 = \frac{k_0 K U_\infty Pe}{\mu a^3}$ for which $Da = \frac{K}{a^2}$ and $Ra = \frac{gK\beta(T_w - T_\infty)a}{\alpha_m v}$, obtained

$$u = \Gamma\frac{\partial^2 u}{\partial y^2} + \frac{k}{\mu}U_\infty \sin x\cos x + k_1\left[u\frac{\partial^3 u}{\partial x\partial y^2} + v\frac{\partial^3 u}{\partial y^3} - \frac{\partial u}{\partial y}\frac{\partial^2 u}{\partial x\partial y} + \frac{\partial u}{\partial x}\frac{\partial^2 u}{\partial y^2}\right] + \lambda\theta\ \sin\ x, \tag{A2}$$

Next, differentiate (A2) with respect to y will yield

$$\frac{\partial\, u}{\partial\, y} = \Gamma\,\frac{\partial^3 u}{\partial\, y^3} + k_1\left[\begin{array}{l} u\frac{\partial^4 u}{\partial x\partial y^3} + \frac{\partial^3 u}{\partial x\partial y^2}\frac{\partial u}{\partial y} + v\frac{\partial^4 u}{\partial y^4} + \frac{\partial^3 u}{\partial y^3}\frac{\partial v}{\partial y} - \frac{\partial u}{\partial y}\frac{\partial^3 u}{\partial x\partial y^2} \\ -\frac{\partial^2 u}{\partial x\partial y}\frac{\partial^2 u}{\partial y^2} + \frac{\partial u}{\partial x}\frac{\partial^3 u}{\partial y^3} + \frac{\partial^2 u}{\partial y^2}\frac{\partial^2 u}{\partial x\partial y}\end{array}\right] + \lambda\,\frac{\partial\,\theta}{\partial\, y}\ \sin\ x, \tag{A3}$$

Non-similarity transformation

By introducing the variables in Equation (12), u and v can be derived as:

$$u = x\frac{\partial f}{\partial y}, v = -x\frac{\partial f}{\partial x} - f, \tag{A4}$$

Integrating Equation (A3), we obtain

$$u = \Gamma\frac{\partial^2 u}{\partial y^2} + k_1\left[u\frac{\partial^3 u}{\partial x\partial y^2} + v\frac{\partial^3 u}{\partial y^3} - \frac{\partial u}{\partial y}\frac{\partial^2 u}{\partial x\partial y} + \frac{\partial u}{\partial x}\frac{\partial^2 u}{\partial y^2}\right] + (1 + \lambda\theta)\ \sin\ x, \tag{A5}$$

In order to make the differentiation process simpler, several derivatives are obtained from (A4) and Equation (A5) becomes

$$\frac{\partial f}{\partial y} = \Gamma\,\frac{\partial^3 f}{\partial\, y^3} + k_1\left[\begin{array}{l} x\frac{\partial f}{\partial y}\frac{\partial^4 f}{\partial x\partial y^3} + \frac{\partial f}{\partial y}\frac{\partial^3 f}{\partial y^3} - x\frac{\partial f}{\partial x}\frac{\partial^4 f}{\partial y^4} - f\frac{\partial^4 f}{\partial y^4} \\ -x\frac{\partial^2 f}{\partial y^2}\frac{\partial^3 f}{\partial x\partial y^2} - \frac{\partial^2 f}{\partial y^2}\frac{\partial^2 f}{\partial y^2} + x\frac{\partial^2 f}{\partial x\partial y}\frac{\partial^3 f}{\partial y^3} + \frac{\partial f}{\partial y}\frac{\partial^3 f}{\partial y^3}\end{array}\right] + (1 + \lambda\theta)\,\frac{\sin\ x}{x}. \tag{A6}$$

Equation (A6) can be simplified as Equation (13).

References

1. Okpara, P.; Ogedengbe, E.; Rosen, M. Effects of velocity and thermal boundary layer with sustainable thermal control across flat plates. *World Sustain. Forum 2014* **2014**, *2014*, 1–12.
2. Jaiswal, B.R. A non-Newtonian liquid sphere embedded in a polar fluid saturated porous medium: Stokes flow. *Appl. Math. Comput.* **2018**, *316*, 488–503. [CrossRef]
3. Kumari, P.; Nigam, M.; Kumar, S.; Kumar, V.; Raturi, S.; Pargaei, M.; Krishna Murthy, S.V.S.S.N.V.G.; Ratish Kumar, B.V. Magnetic field effect on non-darcy mixed convection from a horizontal plate in a nanofluid-saturated porous medium. *J. Porous Media* **2019**, *22*, 599–610. [CrossRef]
4. Malarselvi, A.; Bhuvaneswari, M.; Sivasankaran, S.; Ganga, B.; Abdul Hakeem, A.K. Effect of slip and convective heating on unsteady MHD chemically reacting flow over a porous surface with suction. *Trends Math.* **2019**, *2*, 357–365.
5. Kasim, A.R.M.; Admon, M.A.; Shafie, S. Free convection boundary layer flow of a viscoelastic fluid in the presence of heat generation. *World Acad. Sci. Eng. Technol.* **2011**, *5*, 227–234.
6. Mohamed, M.K.A.; Salleh, M.Z.; Noar, N.A.Z.M.; Ishak, A. The viscous dissipation effects on the mixed convection boundary layer flow on a horizontal circular cylinder. *J. Teknol.* **2016**, *4*, 73–79. [CrossRef]
7. Mahat, R.; Rawi, N.A.; Kasim, A.R.M.; Shafie, S. Mixed convection flow of viscoelastic nanofluid past a horizontal circular cylinder with viscous dissipation. *Sains Malays.* **2018**, *47*, 1617–1623. [CrossRef]

8. Sundar Raju, B.H.; Nath, D.; Pati, S.; Baranyi, L. Analysis of mixed convective heat transfer from a sphere with an aligned magnetic field. *Int. J. Heat Mass Transf.* **2020**, *162*, 120342. [CrossRef]
9. Acrivos, A. On the combined effect of forced and free convection heat transfer in laminar boundary layer flows. *Chem. Eng. Sci.* **1966**, *21*, 343–352. [CrossRef]
10. Merkin, J.H. Mixed convection from a horizontal circular cylinder. *Int. J. Heat Mass Transf.* **1977**, *20*, 73–77. [CrossRef]
11. Ali, A.; Amin, N.; Pop, I. Unsteady mixed convection boundary layer from a circular cylinder in a micropolar fluid. *Int. J. Chem. Eng.* **2010**, *2010*, 417875. [CrossRef]
12. Kasim, A.R.M.; Mohammad, N.F.; Shafie, S. Effect of heat generation on free convection boundary layer flow of a viscoelastic fluid past a horizontal circular cylinder with constant surface heat flux. *AIP Conf. Proc.* **2012**, *1450*, 286–292.
13. Zokri, S.M.; Arifin, N.S.; Mohamed, M.K.A.; Salleh, M.Z.; Kasim, A.R.M.; Mohammad, N.F. Numerical solution on mixed convection boundary layer flow past a horizontal circular cylinder in a Jeffrey fluid with constant heat flux. In Proceedings of the AIP Conference, Kuala Terengganu, Malaysia, 7 August 2017.
14. Zokri, S.M.; Arifin, N.S.; Mohamed, M.K.A.; Kasim, A.R.M.; Mohammad, N.F.; Salleh, M.Z. Mathematical model of mixed convection boundary layer flow over a horizontal circular cylinder filled in a Jeffrey fluid with viscous dissipation effect. *Sains Malays.* **2018**, *47*, 1607–1615. [CrossRef]
15. Mahat, R.; Shafie, S.; Januddi, F. Numerical analysis of mixed convection flow past a symmetric cylinder with viscous dissipation in viscoelastic nanofluid. *CFD Lett.* **2021**, *13*, 12–28. [CrossRef]
16. Basha, H.T.; Sivaraj, R.; Prasad, V.R.; Beg, O.A. Entropy generation of tangent hyperbolic nanofluid flow over a circular cylinder in the presence of nonlinear Boussinesq approximation: A non-similar solution. *J. Therm. Anal. Calorim.* **2021**, *143*, 2273–2289. [CrossRef]
17. Modather, M.; Rashad, A.M.; Chamkha, A.J. An analytical study of MHD heat and mass transfer oscillatory flow of a micropolar fluid over a vertical permeable plate in a porous medium. *Turk. J. Eng. Environ. Sci.* **2009**, *33*, 245–257.
18. Chamkha, A.J.; Khaled, A.A. Hydromagnetic combined heat and mass transfer by natural convection from a permeable surface embedded in a fluid-saturated porous medium. *Int. J. Numer. Methods Heat Fluid Flow* **2000**, *10*, 455–477. [CrossRef]
19. Chamkha, A.J. Non-Darcy hydromagnetic free convection from a cone and a wedge in porous media. *Int. Commun. Heat Mass Transf.* **1996**, *23*, 875–887. [CrossRef]
20. Alrabaiah, H.; Bilal, M.; Khan, M.A.; Muhammad, T.; Legas, E.Y. Time fractional model of electro-osmotic Brinkman-type nanofluid with heat generation and chemical reaction effects: Application in cleansing of contaminated water. *Sci. Rep.* **2021**, *11*, 24402. [CrossRef]
21. Brinkman, H.C. On the permeability of media consisting of closely packed porous particles. *Appl. Sci. Res.* **1949**, *1*, 81–86. [CrossRef]
22. Varma, S.; Babu, M. A Brinkman model for MHD viscous incompressible flow through a porous channel. *Indian J. Pure Appl. Math.* **1985**, *16*, 796–806.
23. Tham, L.; Nazar, R. Numerical solution of mixed convection flow about a sphere in a porous medium saturated by a nanofluid: Brinkman model. *J. Sci. Technol.* **2012**, *4*, 35–46.
24. Yadav, D. The onset of Darcy-Brinkman convection in a porous medium layer with vertical throughflow and variable gravity field effects. *Heat Transf.* **2020**, *49*, 3161–3173. [CrossRef]
25. Rafique, K.; Anwar, M.I.; Misiran, M.; Khan, I.; Sherif, E.S.M. The implicit Keller box scheme for combined heat and mass transfer of Brinkman-type micropolar nanofluid with Brownian motion and thermophoretic effect over an inclined surface. *Appl. Sci.* **2020**, *10*, 280. [CrossRef]
26. Alkasasbeh, H.T.; Salleh, M.Z.; Nazar, R. Mixed convection boundary layer flow about a solid sphere with convective boundary conditions. *Wulfenia J.* **2014**, *21*, 386–404.
27. Ramesh, G.K.; Chamkha, A.J.; Gireesha, B.J. Boundary layer flow past an inclined stationary/moving flat plate with convective boundary condition. *Afrika Mat.* **2016**, *27*, 87–95. [CrossRef]
28. Sarif, N.M.; Salleh, M.Z.; Nazar, R. Mixed convection flow over a horizontal circular cylinder in a viscous fluid at the lower stagnation point with convective boundary conditions. *ScienceAsia* **2016**, *42*, 5–10. [CrossRef]
29. Sarif, N.M.; Salleh, M.Z.; Nazar, R. Mixed convection over a horizontal circular cylinder embedded in porous medium immersed in a nanofluid with convective boundary conditions at lower stagnation point: A numerical solution. In Proceedings of the MATEC Web Conference, Beijing, China, 25–27 May 2018.
30. Bilal Ashraf, M.; Hayat, T.; Alsaedi, A. Mixed convection flow of Casson fluid over a stretching sheet with convective boundary conditions and Hall effect. *Bound. Value Probl.* **2017**, *2017*, 1–17. [CrossRef]
31. Mahat, R.; Afiqah, N.; Kasim, A.R.M.; Shafie, S. Heat generation effect on mixed convection flow of viscoelastic nanofluid: Convective boundary condition solution. *Malays. J. Fundam. Appl. Sci.* **2020**, *16*, 166–172. [CrossRef]
32. Tonekaboni, S.A.; Abkar, R.; Khoeilar, R. On the Study of Viscoelastic Walters' B Fluid in Boundary Layer Flows. *Math. Probl. Eng.* **2012**, *2012*, 861508. [CrossRef]
33. Nazar, R.; Amin, N.; Filip, D.; Pop, I. The Brinkman model for the mixed convection boundary layer flow past a horizontal circular cylinder in a porous medium. *Int. J. Heat Mass Transf.* **2003**, *46*, 3167–3178. [CrossRef]
34. Aziz, L.A.; Kasim, A.R.M.; Salleh, M.Z. Development on mathematical model of convective boundary layer flow of viscoelastic fluid with microrotation effect under constant wall temperature thermal condition over a bluff body. *ASM Sci. J.* **2019**, *12*, 86–90.

35. Tham, L.; Nazar, R.; Pop, I. Mixed convection boundary layer flow past a horizontal circular cylinder embedded in a porous medium saturated by a nanofluid: Brinkman model. *J. Porous Media* **2013**, *16*, 445–457. [CrossRef]
36. Yirga, Y.; Shankar, B. MHD flow and heat transfer of nanofluids through a porous media due to a stretching sheet with viscous dissipation and chemical reaction effects. *Int. J. Comput. Methods Eng. Sci. Mech.* **2015**, *16*, 275–284. [CrossRef]
37. Shafie, S.; Saqib, M.; Khan, I.; Qushairi, A. Mixed Convection Flow of Brinkman Type Hybrid Nanofluid Based on Atangana-Baleanu Fractional Model. *J. Phys. Conf. Ser.* **2019**, *1366*, 012041. [CrossRef]